J Comput Aided Mol Des (2006) 20:395–404
DOI 10.1007/s10822-006-9081-z

ORIGINAL PAPER

Molecular dynamics simulations on the inhibition of Cyclin-Dependent Kinases 2 and 5 in the presence of activators

Bing Zhang · Vincent B. C. Tan · Kian Meng Lim · Tong Earn Tay

Received: 20 May 2006 / Accepted: 18 September 2006 / Published online: 13 October 2006

Abstract Interests in CDK2 and CDK5 have stemmed mainly from their association with cancer and neuronal migration or differentiation related diseases and the need to design selective inhibitors for these kinases. Molecular dynamics (MD) simulations have not only become a viable approach to drug design because of advances in computer technology but are increasingly an integral part of drug discovery processes. It is common in MD simulations of inhibitor/CDK complexes to exclude the activator of the CDKs in the structural models to keep computational time tractable. In this paper, we present simulation results of CDK2 and CDK5 with roscovitine using models with and without their activators (cyclinA and p25). While p25 was found to induce slight changes in CDK5, the calculations support that cyclinA leads to significant conformational changes near the active site of CDK2. This suggests that detailed and structure-based inhibitor design targeted at these CDKs should employ activator-included models of the kinases. Comparisons between P/CDK2/cyclinA/roscovitine and CDK5/p25/roscovitine complexes reveal differences in the conformations of the glutamine around the active sites, which may be exploited to find highly selective inhibitors with respect to CDK2 and CDK5.

Keywords Cyclin-dependent kinase · Drug design · Inhibitors · Molecular dynamics · Selectivity

Abbreviations

(CDK)	Cyclin-Dependent Kinase
P/CDK2/cyclinA/roscovitine	Thr160–phosphated/CDK2/cyclinA/roscovitine

Introduction

Both Cyclin-Dependent Kinase 2 (CDK2) and Cyclin-Dependent Kinase 5 (CDK5) have generated a marked interest among cell biologists, neuroscientists and biochemists. CDK2 is targeted in cancer therapy due to its role in cell division cycle [1–3] while CDK5 presents an attractive pharmacological target because its deregulation is implicated in various neurodegenerative diseases such as Alzheimer's disease, Parkinson's disease, etc [4–8]. Compared to the level of interest in CDK2, less attention has been paid to the activity of compounds involved in non-cell-cycle-control related CDKs, like CDK5.

CDK2 and CDK5 belong to a large family of heterodimeric serine/threoine protein kinases comprising a catalytic CDK subunit and an activating subunit [1, 9–13]. The subunits of these CDKs have very similar 3-dimensional structures as reflected in their sequence

B. Zhang · V. B. C. Tan · K. M. Lim · T. E. Tay
Nanoscience and Nanotechnolgy Initiative, National University of Singapore, S117576 Singapore, Singapore

V. B. C. Tan (✉) · K. M. Lim · T. E. Tay
Department of Mechanical Engineering, National University of Singapore, S117576 Singapore, Singapore
e-mail: mpetanbc@nus.edu.sg

B. Zhang
Department of Chemistry, Zhejiang University, Hangzhou 310027, P.R. China

identity of 60%. Both these kinases are folded into a typical bilobal conformation. They have an N-terminal domain of approximately 85 residues in a mainly β-sheet structure, a predominantly α-helix C-terminal domain of about 170 amino acids and a deep ATP-binding cleft between the two lobes. Despite their similarities, the activating subunits of CDK2 and CDK5 are different.

CyclinA, the activator of CDK2, has a globular structure consisting of 12 α-helices [14]. Residues 209–310 of cyclinA fold into a well-conserved globular domain among cyclins known as the Cyclin-Box Fold (CBF). The CBF is in contact with the activating loop (T-loop) of CDK2 and is the crucial segment at the cyclinA-CDK2 interface, which forms the binding site for the PSTAIRE helix. CDK5 can be activated by p35 or just the proteolytic p25 segment of p35 containing the C-terminal portion [15–17]. Compared to its unstable p35 parent activator, p25 displays a substantially longer half-life. Residues 147–293 of p25 form a Cyclin-Box Like Fold (CBFL) domain, which binds CDK5 around the PSAALRE helix and the activation loop (T-Loop).

The relative position of the CBFL domain to CDK5 is similar to that occupied by the CBF in cyclinA when it is bound to CDK2. Although the CDK5/p25 and CDK2/cyclinA complexes are structurally very similar to each other, there are still detailed yet important structural and regulatory differences between these two systems [17]. Association with cyclinA and phosphorylation on Thr160 are required for complete activation of CDK2 [14, 18]. However, only an association with p25 is enough to fully activate CDK5 [17]. Conformational changes that take place during the activation of CDK2 to create the substrate binding site and correctly orientate residues required for ATP binding and subsequent phosphotransfer have been well documented [14, 18, 19]. However, similar reports on the activation of CDK5 are lacking because the structure of apo CDK5 is still unknown.

In the past decade, several theoretical studies on CDKs based on both molecular dynamic simulations and quantum mechanical calculations [20–29] have been carried out to supplement the abundance of experimental works. However, most simulations are based solely on monomeric CDK templates and do not take into account the activators. More recently, Davies et al. [30] questioned the validity of using the monomeric CDK2 as a model for the active kinase in structure-based drug design because they suspect that the accuracy of monomeric CDK2 as an inhibitor design template is restricted to the adenine binding site.

Although specific inhibition of a protein kinase is highly desirable, it remains a challenging goal in drug design [31–34]. In the past decade, many ATP-competitive inhibitors of cell cycle control related CDKs have been suggested [32, 35–39] and several of them have progressed to clinical trials targeting diverse types of cancer. Unfortunately, none has yet been approved for use in cancer therapy partly because of the lack of clean inhibition of single targeted CDKs [34]. Despite their different pathological roles, highly selective inhibitors of CDK2 and CDK5 have yet to be discovered.

Dynamical studies on binding modes are necessary to understand key structural features and interactions to provide valuable information for the design of efficient inhibitors. Roscovitine [1-ethyl-2-hydroxyethylamino)-6-benzylamino-9-isopropylpurine] (Fig. 1) is a purine analog that has been shown to potently inhibit CDKs with inhibitory concentration (IC_{50}) values ranging from 0.16 μM (for CDK5), 0.70 μM (for CDK2) to over 100 μM (for CDK4 and CDK6) while maintaining good selectivity with respect to a number of other kinases [40–42]. However, the selectivity between CDK2 and CDK5 is still far from ideal. Here, we give detailed results of four molecular dynamics simulations on apo-CDK2, Thr160-phosphated/CDK2/cyclinA/roscovitine (referred to as P/CDK2/cyclinA/roscovitine hereafter), apo-CDK5 and CDK5/p25/roscovitine. By comparing these results with our previous simulations on CDK2/roscovitine and CDK5/roscovitine, the significance of the influence of the activators on the inhibitor-kinase binding mode is revealed. Our results clearly suggest that fully active CDKs should be used as the structure-based drug design template instead of apo-CKDs. Comparisons of the conformations of residues lining the active sites of all the complexes and an energy decomposition study have led to some important ideas on potent selective inhibitor design.

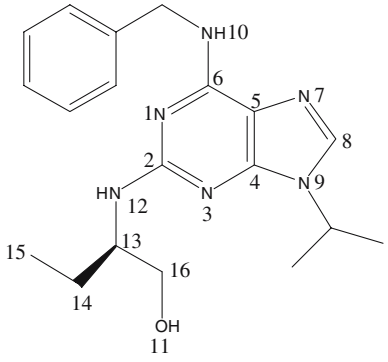

Fig. 1 Molecular structure of roscovitine under investigation

Materials and methods

Molecular dynamics simulations

Molecular dynamics simulations were carried out using the SANDER module of AMBER 8.0 with the Cornell et al. all-atom force field [43]. Prior to the MD simulations, the values for some of the force field parameters for the ligands had to be developed because of the lack of reported data. Optimization of the five ligands were first achieved with the Gassuian98 package at the HF/6–31G* theoretical level. Electrostatic potentials (ESP) were then generated with Merz–Singh–Kollman van der Waals parameters [44]. Fitting of the charges to the ESP was performed with the RESP program [45] of the AMBER package. GAFF [46] force fields parameters and RESP partial charges were assigned using the ANTECHAMBER module.

The starting geometries for the simulations of apo CDK2 and CDK5/p25/R-roscovitine were generated from X-ray structures obtained from the Protein Data Bank (PDB ID code: 1PW2, 1UNL, respectively) while the crystal structure of CDK2/R-roscovitine was kindly provided by Prof. Laurent Meijer and Dr. Sung-Hou KIM (CNRS, Station Biologique, France, University of Berkeley, the U.S., respectively). Both apo CDK5 and CDK5/roscovitine are modified from CDK5/p25/R-roscovitine by simply removing the inhibitor and the activator. The initial structure of the P/CDK2/cyclinA/roscovitine was derived from an autodock simulation. All simulations are at neutral PH, Lys and Arg residues are positively charged and Asp and Glu residues are negatively charged. The default His protonation state in Amber8 is adopted. Counter ions were added to maintain the eletroneutrality of all the systems. Each system was immersed in a 10 Å layer truncated octahedron periodic water box. The layer of water molecule in all cases contained around 11,000 TIP3P [47] water molecules in each of the complexes. A 2 fs time step was used in all the simulations and long-range electrostatic interactions were treated with the particle mesh Ewald (PME) procedure [48] using a cubic B-spline interpolation and a 10^{-5} tolerance for the direct-space and with a 12 Å non-bonded cutoff. Bond lengths involving hydrogen atoms were constrained using the SHAKE algorithm [49]. All systems were minimized prior to the production run. The minimization, performed with the SANDER module under constant volume condition, consists of 7 steps. All heavy atoms in both proteins and ligands were restrained with degressive forces of 500, 200, 100, 50, 5, 1 kcal/mol, respectively. In the first 3 steps, minimization of the solvent molecules and hydrogen atoms of the systems involved 250 cycles of steepest descent followed by 250 cycles of conjugated gradient minimization. In the next 3 steps, 100 cycles of steepest descent minimization were performed followed by 500 cycles of conjugated gradient minimization. All systems were then relaxed by 500 cycles of steepest descent and 1,000 cycles of conjugated gradient minimization. After the relaxation, the systems were heated to 300 K. The production part of all the systems spanned 2ns.

Automated molecular docking

To effect the docking of roscovitine onto the activated CDK2, a P/CDK2/cyclinA/4-(6-cyclohexylmethoxy-9H-purin-2-ylamino)-benzamide complex was first aligned with the CDK2/roscovitine complex. The CDK2 in the latter complex and the inhibitor in the former system were then excluded and the position of roscovitine in the P/CDK2/cyclinA was used as the initial position for docking. In this docking simulation, we used the AutoDock 3.0 program [50]. The Lamarckian genetic algorithm (LGA) [51] was employed to treat the inhibitor–protein interactions. The number of generations, energy evaluations and docking runs were set to 50,000, 1,500,000 and 20, respectively. Of all the conformations obtained from the docking runs, only those with positional root mean square deviation less than 1.5 Å were accepted. The conformation of the docked complex with the lowest energy was used for the analysis reported in this paper.

Molecular Mechanics-Possion–Boltzmann/Surface Area (MM-PBSA) analysis

Results were analyzed using the PTRAJ module in AMBER. An energy decomposition method was performed using the MM-PBSA (Molecular Mechanics-Possion–Boltzmann/Surface Area) [52] approach in the AMBER8.0 package to partition electrostatic and van der Waals energy contributions between active site residues. In this method, the binding free energy is decomposed into contributions from molecular mechanics energy, nonploar and electrostatic solvation free energies and relative solute energy effects. Binding free energies of all the systems were analyzed using the MM-PBSA approach to highlight the electrostatic and van der Waal contributions in the binding of the inhibitors and the proteins.

The binding free energies (ΔG_{bind}) were computed as:

$$\Delta G_{\text{bind}} = \Delta G(\text{complex}) - [\Delta G(\text{protein}) + \Delta G(\text{ligand})] \quad (1)$$

$$\Delta G_{\text{bind}} = \Delta E_{\text{gas}} + \Delta\Delta G_{\text{solv}} - T\Delta S \quad (2)$$

$$\Delta E_{\text{gas}} = \Delta E_{\text{int}} + \Delta E_{\text{ele}} + \Delta E_{\text{vdw}} \quad (3)$$

$$\Delta G_{\text{solv}} = \Delta G_{\text{pb}} + \Delta G_{\text{non-polar}} \quad (4)$$

The sum of molecular mechanical energies, ΔE_{gas}, can be divided into contributions from internal energy (ΔE_{int}), electrostatic potential (ΔE_{ele}) and van der Waals (ΔE_{vdw}) potential. The solvation free energy (ΔG_{solv}) is composed of two parts—polar solvation free energy (ΔG_{PB}) and non-polar solvation free energy ($\Delta G_{\text{non-polar}}$). All energies are averaged along the MD trajectories. E_{gas} was obtained using SANDER and an estimation of ΔG_{PB} was calculated with a built-in module, PBSA in AMBER. $G_{\text{non-polar}}$ was determined from Eq. 4 using the MOLSURF program [53, 54].

$$\Delta G_{\text{non-polar}} = 0.00542\text{SASA} + 0.92 \quad (5)$$

Results and discussion

NPT MD simulations were performed separately on complexes of CDKs with the activators and the inhibitors. The root-mean-squared deviations (RMSD) fluctuations of backbone atoms compared to the X-ray structures were obtained over a 2ns NPT trajectory. The RMSD of the CDK2 and CDK5 systems in Figure 2 indicates that the solvated systems had attained equilibrium after some initial fluctuations. Because the structures of apo CDK5 and monomeric CDK5 complex with roscovitine are unavailable, only a comparison of the calculated temperature B-factors of the CDK2/roscovitine and the P/CDK2/cyclinA/roscovitine is presented. As shown in Fig. 3, the cyclinA binding increases the stability of the PSTAIRE helix (residues 46–56) and the activation loop (residue 153–164) significantly and decreases thermal movements in these regions by direct interactions. This stabilization, which has been reported in several crystallographic studies [14], serves as one measure of verification of the molecular dynamics simulations.

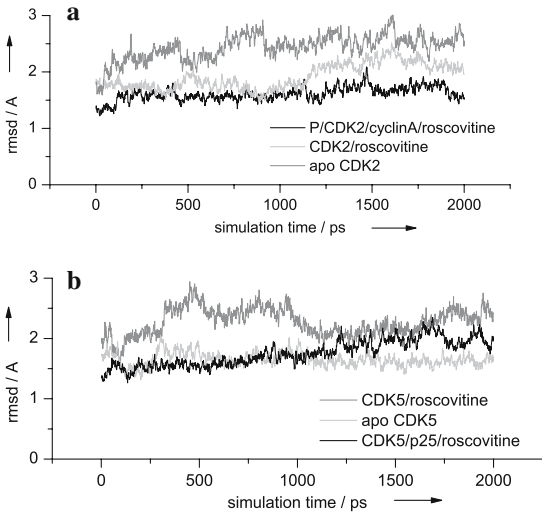

Fig. 2 Time dependence of the root mean square deviations from starting structures for: (**a**) CDK2, and (**b**) CDK5 complexes with activators and inhibitors under investigation

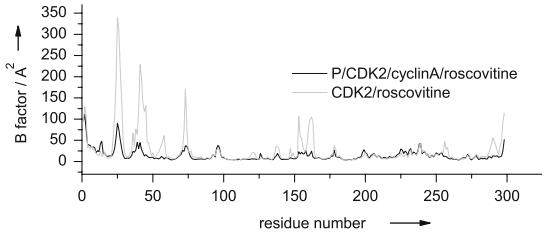

Fig. 3 B-factors of CA atoms of CDK2 in CDK2/roscovitine and P/CDK2/cyclinA/roscovitine

Binding patterns

The calculations suggest that inhibitors bind predominantly in the region of the pocket occupied by the ATP adenine ring in all the complexes and form hydrogen bonds with the backbone of the CDKs at the hinge region (Table 1). Two crucial hydrogen bonds (HB) listed in Table 1, N^{10}–H···O (Leu83 in CDK2, Cys83 in CDK5) and N^{7}···H–N (Leu83 in CDK2, Cys83 in CDK5) were found in our simulations for both the CDK5 and CDK2 complexes (Fig. 4). These bonds have been reported to play a key role in the binding of roscovitine with CDK2 and CDK5 [13]. In addition to these two bonds, another single HB, O^{11}–H···O (Gln131 in CDK2, Gln130 in CDK5), was found in CDK2/roscovitine, CDK5/roscovitine and CDK5/p25/roscovitine. This bond, however, is not found in the P/CDK2/cyclinA/roscovitine complex. This means that the binding mode of roscovitine with CDK5 is similar with or without the activator but the binding pattern in CDK2 cannot be correctly reflected if its activator is excluded in the MD simulations.

Table 1 Hydrogen bonds between the inhibitors and the active sites as obtained from simulations

Complex	Hydrogen bond	Duration[a]	Mean distance (Å)[b]	Mean angle (°)
CDK5/R–roscovitine	$N^{10}H\cdots O$(Cys83)	94.57	2.93	39.98
	$N^{7}\cdots HN$(Cys83)	88.82	3.20	27.68
	$O^{11}H\cdots O$(Gln130)	84.38	2.73	21.45
CDK2/R–roscovitine	$N^{10}H\cdots O$(Leu83)	99.20	2.93	35.06
	$N^{7}\cdots HN$(Leu83)	80.93	3.24	22.11
	$O^{11}H\cdots O$(Gln131)	95.53	2.68	17.24
CDK5/p25/S–roscovitine	$N^{10}H\cdots O$(Leu83)	97.96	2.97	40.70
	$N^{7}\cdots HN$(Leu83)	72.34	3.27	28.96
	$O^{11}H\cdots O$(Gln130)	97.60	2.73	15.35
P/CDK2/cyclinA/roscovitine	$N^{10}H\cdots O$(Leu83)	96.25	2.99	39.05
	$N^{7}\cdots HN$(Leu83)	75.45	3.53	22.43
	$O^{11}\cdots HNE2$(Gln131)	12.00	3.04	28.22
	$O^{11}H\cdots O$(Glu12)	43.10	2.75	20.78
	$O^{11}H\cdots O$(Ile10)	20.00	2.75	17.21

[a] Percentage of equilibration simulation time. [b]The hydrogen bond distances are heavy atom distances

A close look at the binding mode in the averaged structures shows that in the absence of cyclinA and the phosphated Thr160, the two torsions (N^{12}–C^{13}–C^{14}–C^{15} and N^{12}–C^{13}–C^{16}–O^{11}) at the C2 side chain of the roscovitine rotate to form the additional HB between O^{11}–H and the backbone oxygen of Gln131. In both a previous 1ns NVT simulation [21] and our own MD simulations on the CDK2/roscovitine complex, the rotation of these two torsions were also detected. However, our results reveal that these rotations do not take place when the activator and phosphorylating the Thr160 are included in the simulations.

The absence of the rotation in the fully activated CDK2 system means that the activated CDK2 and activated CDK5 have considerably different conformation near the active site. This has implications on the way inhibitors bind with the two different CDKs. The differences of the binding modes among these complexes are significant because they do not only implicate the importance of the influence from the activator but also the potential to improve the selectivity of the purine analogue inhibitor.

Torsional rotation of N^{1}–C^{2}–N^{12}–H^{N12}

It can be seen from the 3D structure of the roscovitine that any rotation of the substituents on the C2 side will experience steric hindrance from either the big benzyl on N^{10} or the isopropyl on N^{9}, because during the simulations, it was detected that the flexibility of the benzyl and the isopropyl group is partially restricted due to the interactions from the kinase. A potential surface scan of the torsion angle N^{1}–C^{2}–N^{12}–H^{N12} on the roscovitine was preformed to determine the energy barrier of the rotation, to mimic the semi-rigid conformation of the inhibitor in the complex; both the benzyl group and the isopropyl group are partially fixed. The surface scan was performed using the Gaussian98 package at the b3lyp/6-31G* theoretical level. As seen in Fig. 5, minimum energy conformations occur when the torsion angle of N^{1}–C^{2}–N^{12}–H^{N12} is around ±165° or 0°. These correspond to conformations when the plane constituted by C^{14}–C^{13}–C^{16} is almost perpendicular to the purine ring plane, which is when the molecule has the most stable conformation.

The torsion angles of N^{1}–C^{2}–N^{12}–H^{N12} in the averaged CDK5/p25/roscovitine, CDK5/roscovitine, P/CDK2/cyclinA/roscovitine and CDK2/roscovitine complexes are 163.2° 169.0°, 0.7° and 170.2°, respectively. Hence, the inhibitors present very stable structures in all the averaged systems albeit with different conformations. Figure 5 also implies that from one minimum energy conformation to another, the rotation of the substituent on the C2 chain has to overcome an energy barrier of up to 18 kcal/mol. This is nevertheless a moderate barrier to overcome, especially in the CDK2/roscovitine system, where a stable hydrogen bond between the hydroxyl group on C^{16} and backbone oxygen of the Gln131 is established after the rotation of the roscovitine. Such a rotation, however, does not occur in the activated in the CDK2 system. While informative, an analysis of the energy barrier inside the inhibitor by itself does not provide enough information on why no rotation occurs.

Influence of CDK activators

It is well known that the binding site of the inhibitors is in the ATP adenine ring-binding pocket formed by the small N-terminal lobe and the larger C-terminal lobe [14]. Both the glycine-rich inhibitory loop (G-Loop) comprising residues 11–18, and the DFG motif (resi-

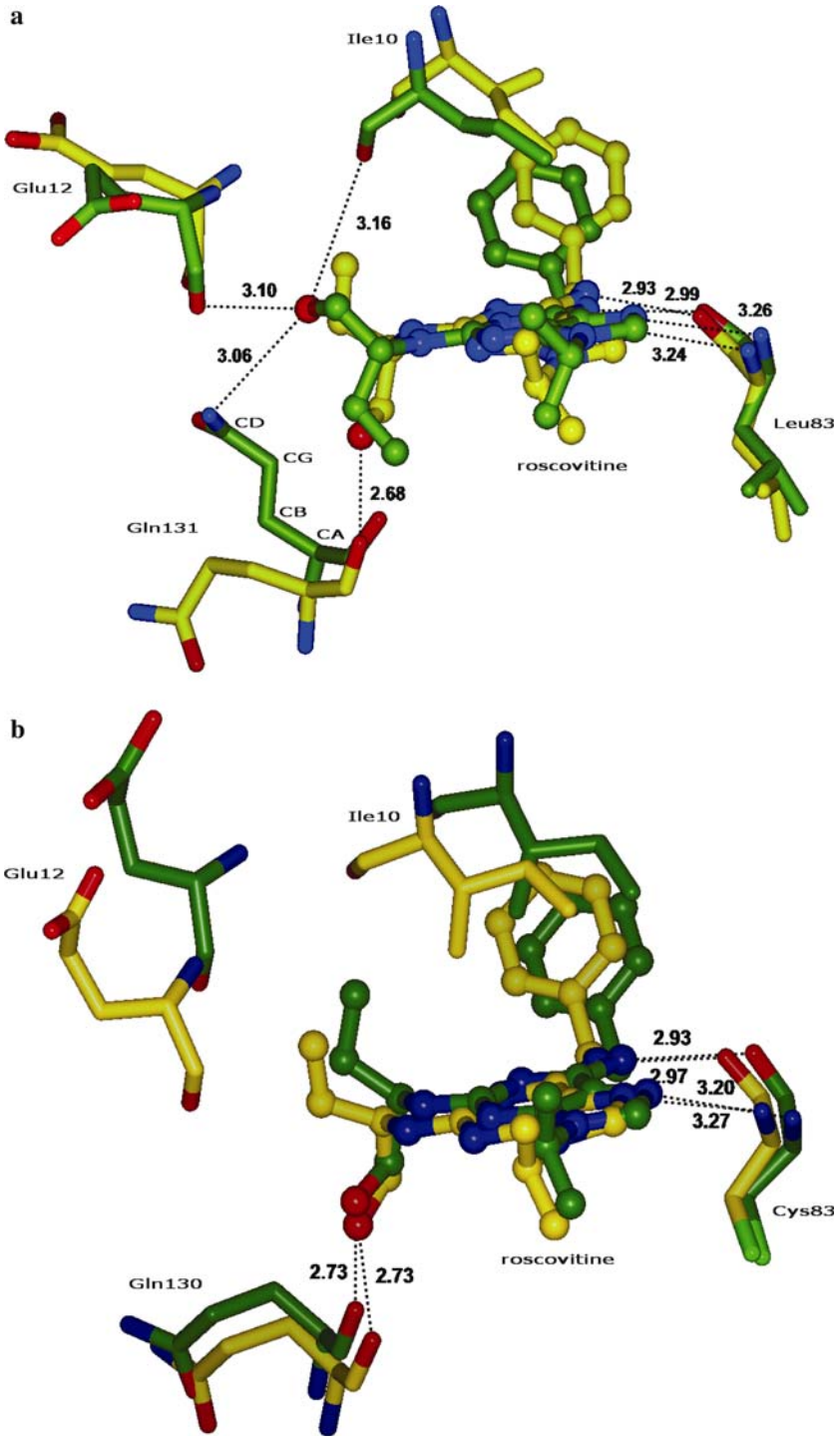

Fig. 4 HB networks around the active sites of: (**a**) CDK2/roscovitine (yellow) and P/CDK2/cyclin/roscovitine (green), and (**b**) CDK5/roscovitine (yellow) and CDK5/p25/roscovitine (green). In this figure, oxygen atoms are in red and nitrogen in blue

dues 145–147, from the single-letter amino acid code) connected in front of the αL12 helix in inactive CDK2 or the β9 sheet in fully active CDK2 are involved in the ligand binding site. Due to the melting of the αL12 helix to β9 during the activating process, the DFG loop approaches the G-loop. The two loops are comparable to a ''door'' leading to the active site on the activator side. Both the binding of the inhibitor and the activator with the kinase can influence the status of the door.

Figure 6 compares the probability distributions of the distance between the CA atom of Thr14 at the apex of the G-loop and the CA atom of Gly147 in CDK2 systems and the distance between the CA atom of Thr14 and the CA atom of Gly146 in CDK5. It is seen

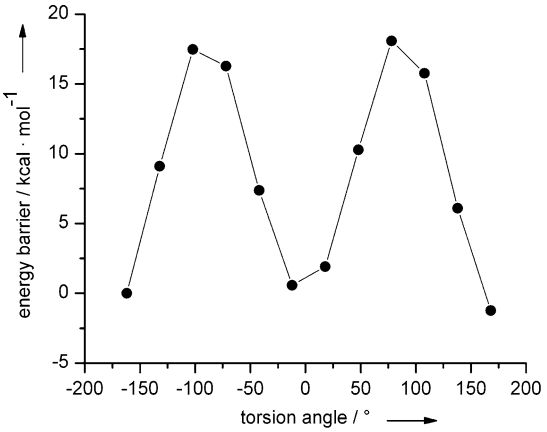

Fig. 5 Potential surface of different conformations of roscovitine

from Fig. 6a that the distance between these two atoms increases from 11.8 Å in apo CDK2 to 12.8 Å in the CDK2/roscovitine complex. This increase in interatomic distance is also observed when CDK5/roscovitine (6.0 Å) is compared to apo CDK5 (5.2 Å) in Fig. 6b. Hence, the ''door'' is widened slightly when the inhibitor is enclosed inside the active site.

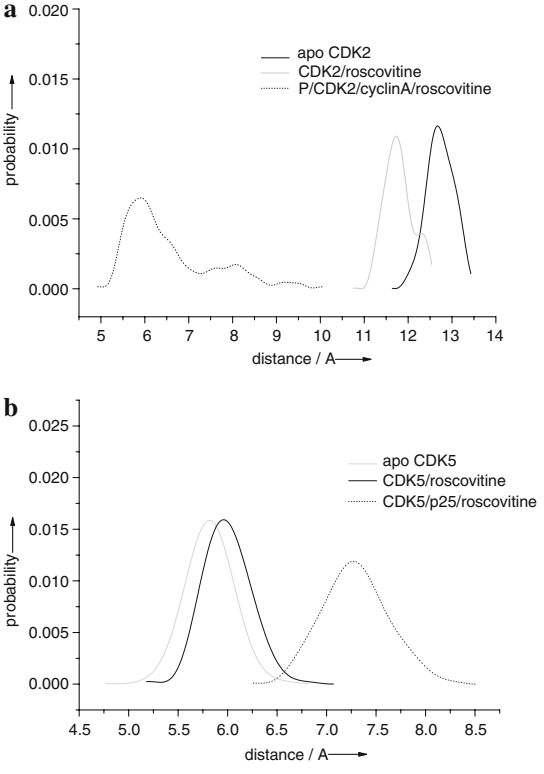

Fig. 6 Probability distribution for the distances: (**a**) between the CA atoms of Thr14 and Gly147 in CDK2, and (**b**) between those of Thr14 and Gly146 in CDK5

However, simulations using monomeric CDK2 and CDK4 complexes with NU6102 like inhibitors [25] have predicted that the distance between the Thr14 in CDK2 (Ala16 in CDK4) and the Gly147 and the distance between the Ala16 in CDK4 and the Gly160 decrease slightly when the inhibitors bind to the kinases. Different results have also been obtained when the activators are included in the simulations. When cyclinA is added to CDK2, the door becomes narrower in the fully active CDK2 (5.8 Å) but when p25 is added to CDK5, the door opens even wider (7.3 Å). This means the inhibitor in the fully active CDK2 is accommodated in a narrower space than that in the active CDK5. The different behaviors of the doors in both the active CDKs can be explained by analyzing the relative positions of the G-loop and the T-loop. As shown in Fig. 7, the G-loop in both systems is located at approximately the same region. However, the T-loop of the CDK5 complex is much lower and wider than that in CDK2. This drags the β sheet and the DFG motif away from the G-loop in opposite directions thereby causing the door to widen.

It has been reported that p25 and the N-terminal region of cyclinA adopt a similar position on their cognate kinases [17]. However, there is more extensive contact between p25 and the activation loop of the CDK5 compared with the interactions between cyclinA and the G-loop of the CDK2. Moreover, the locations of the residues in the activators in contact with the CDKs are different. The interaction of p25 with CDK5 involves residues located outside the cyclin-box-fold-like (CBFL) region whereas the residues involved in the interactions with the G-loop of CDK2 are Phe267, Ile182, Ile270, Glu269, Ile270 and Gln228. These are mostly located on α1–α2 loop and α3–α4 loop in the cyclin-box-fold (CBF) region [14]. Figure 7 shows the two activation loops and the residues in the activators in both active systems. As seen in the figure, the positions of the residues in the CBFL in p25 and those in CBF in cyclin are different and the positions of the p25 residues are slightly lower than the cyclin residues. The residues in the CBFL drag the T-loop in CDK5 further down and stretch it more than the T-loop in CDK2. There is also another reason why the T-loop in CDK2 cannot be as extended as that in CDK5. In CDK2/cyclinA, the αNT terminal of the cyclinA is located just behind the T-loop. Although van der Waals forces could enhance the interactions between the CDK and the activator [14, 17], it also prevents extensive stretching of the activation loop. In the CDK5/p25 complex, there is no such restriction on the movement of the T-loop. As a result, the different T-loop conformations lead to different size of free

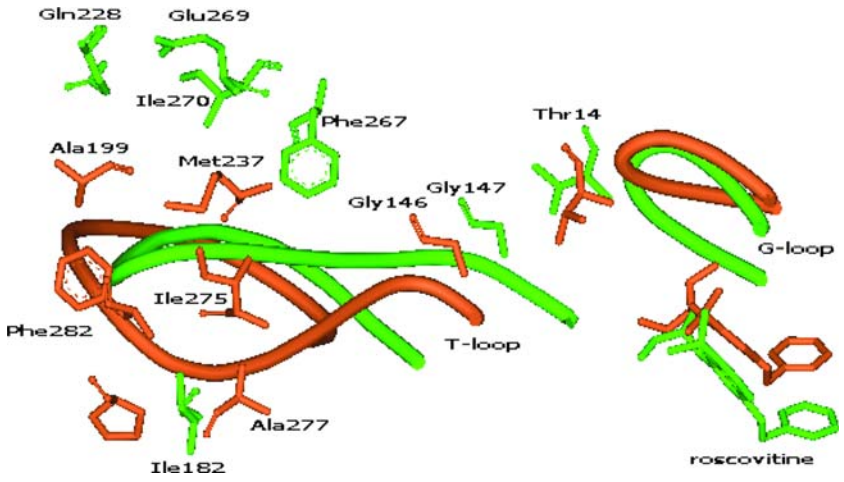

Fig. 7 Relative positions of T-loop and G-loop in both the active kinase complexes. In this figure, all atoms in P/CDK2/cyclinA/roscovitine are in green and those in the CDK5/p25/roscovitine are in orange

space at the active sites. The narrower space in the P/CDK2/cyclinA/roscovitine around the big substituent on the C2 chain makes it difficult for inhibitors to rotate.

Conformation of the glutamine at the active sites

A comparison of the conformations of 20 crucial residues lining the active sites of complexes [13] was made. It was found that the conformation of Gln131 in the P/CDK2/cyclinA/roscovitine differs significantly from that in the apo kinases, the CDK2/roscovitine and in both the CDK5 complexes (Fig. 4). The glutamine creates a hydrogen bond between the backbone oxygen atom and the O^{11}–H of the roscovitine in the CDK2/roscovitine, the CDK5/roscovitine and the CDK5/p25/roscovitine systems (Table 1) and all the conformations are very similar in these complexes. However, in the P/CDK2/cyclinA/roscovitine combination, the side chain of Gln131 does not stretch out of the active site as in the other five systems. It, instead, tilts upward towards the inhibitor. The torsion angle CA-CB-CG-CD in the CDK2/roscovitine and the P/CDK2/cyclinA/roscovitine are 86.3° and 174.5°, respectively.

The behavior of the Gln131 side chain could be very important in explaining the absence of rotation in the P/CDK2/cyclinA/roscovitine and for designing new inhibitors and improving inhibitor selectivity between CDK2 and CDK5. It is apparent from the relative positions of the side chain of the Gln131 and the substituent on the C2 chain of the inhibitor that the new conformation of the side chain of the Gln131 forms a ''wall'' in the front of the substituent. This reorientation of the side chain further narrows the active site and therefore applies more steric hindrance to restrain the movement of the substituent of the inhibitor. The ''wall'' formed by this residue also prevents any substituents from pointing out of the active site. Therefore, the CDK2 active site may not be able to enclose larger groups on the C2 chain as they may clash with the glutamine side chain. However, such hindrance does not exist in the CDK2/roscovitine and the CDK5 complexes, so larger substituents can be considered as possible inhibitors at the C2 site. The different wall orientation may also change the electrostatic interaction pattern between the inhibitor and Gln131. This is supported by an analysis of the hydrogen bonding in both the CDK5/p25/roscovitine and P/CDK2/cyclin/roscovitine complexes shown in Table 1. In the CDK5 complex, a hydrogen bond of length 2.734 Å is observed between the backbone oxygen of Gln130 and O^{11}–H for 98% of the simulation duration. It is one of the most important and strongest electrostatic interactions between the protein and the inhibitor. However, in the fully active CDK2 system, the hydrogen bonding is created between the NE2-H on the Gln131 and the O^{11} of the inhibitor, and the duration and bond length are 12% and 3.035 Å, respectively. Although the duration is short and the bond length is large, this hydrogen bonding is a new electrostatic interaction mode unlike that in the CDK5 complex.

Besides the distinct HB between the glutamine and the inhibitor in the P/CDK2/cyclinA/roscovitine, two other HBs different from those in the CDK5 systems were noticed during our HB analysis. These HBs are also partly responsible for restricting the rotation. As listed in Table 1, one of the HBs is established between the backbone oxygen atom of the Ile10 and the O^{11}–H of the inhibitor and the other between the backbone oxygen atom of the Glu12 and the O^{11}–H. Figure 8 gives the distances between the backbone oxygen and the O^{11}–H. Assuming 2.5 Å as the length defining a HB, as suggested by Lemaitre et al. [55], it is clear that, although the hydrogen on the hydroxyl group can bond to both the backbone oxygen atoms, the HB is not

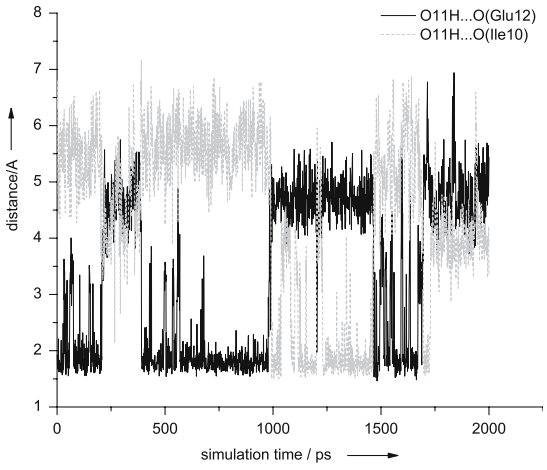

Fig. 8 Calculated distances between the O^{11}–H of the inhibitor and two residues (Glu12 and Ile10) in the P/CDK2/cyclinA/roscovitine complex

bifurcated. It is apparent from the relative positions of Ile10 and Glu12 to the hydroxyl group that these two residues sandwich and, thus, restrict the movement of the group when HBs with the O^{11}–H are formed.

In the examination of amino acids of the active sites, no other significant conformation change has been detected. However, an energy decomposition analysis revealed several amino acids, which interact with the inhibitor with completely opposite electrostatic interactions from those in the CDK2/roscovitine, the P/CDK2/cyclinA/roscovitine and the CDK5/p25/roscovitine complexes. As listed in Table 2, Gly13 and Phe146 in CDK2 (Phe145 in CDK5) exhibit attraction with the roscovitine in the P/CDK2/cyclinA/roscovitine complex but repulsion in the CDK5/p25/roscovitine and the CDK2/roscovitine complexes. The Lys89 repels the inhibitor in both the CDK2 systems but attracts the inhibitor in the CDK5 system. It was also noticed that all the residues are at the same side of the inhibitor and around the hydroxyl group. We believe that the different electrostatic contributions originate from the displacement of the hydroxyl group. For the purpose of improving drug selectivity, it is important to examine interactions with residues exhibiting significant electrostatic contributions to the binding between the inhibitor and the CDK2/CDK5 complexes.

Table 2 Single residue electrostatic contributions to the interaction between the inhibitors and the kinases (in kJ/mol)

Complex	Residue	S^{a}_{ele}	B^{b}_{ele}	T^{c}_{ele}
P/CDK2/cyclinA/roscovitine	Gly13	–4.07	–1.64	–5.71
	Lys89	15.91	–2.11	13.80
	Phe146	0.55	–2.69	–2.14
CDK5/p25/roscovitine	Gly13	–1.56	5.34	3.78
	Lys89	0.47	–4.91	–4.44
	Phe145	1.58	–1.53	0.05

[a] Electrostatic contribution from amino acid side chain

[b] Electrostatic contribution from amino acid backbone

[c] Total electrostatic contribution from amino acid

Conclusion

Different conformations of roscovitine due to the rotation of a substituent on the C2 side chain in monomeric CDK2/roscovitine and fully activated P/CDK2/cyclinA/roscovitine complexes are detected in our simulations. The rotations responsible for the conformational differences have been elucidated in this study by means of a combined computational protocol involving docking experiments, molecular dynamics simulations and MM-PBSA simulations. It was found that no rotation occurs in the fully active CDK2 complex due to four restraints. First, by adding the activator to the CDK2, the active site on the activator side is considerably narrowed compared to the monomeric CDK2. Second, the different conformation of the side chain of the Gln131 in the P/CDK2/cyclinA/roscovitine not only prevents larger substituents from pointing out of the active site, but also exerts additional steric hindrance on the movement of the substituent on the C2 side chain. Thirdly, two residues, which sandwich the substituent, create HBs with the hydroxyl to further restrain its movement. Finally, an up to 18 kcal/mol rotation energy barrier originating from the inside of the inhibitor also helps to confine its rotation. As a result, the conformations of the inhibitor in the inactive and active CDK2 are distinctly different. Correct initial 3D-structures of both protein and its inhibitor are crucial for structural-based drug design. Our investigations suggest that simulations using monomeric CDKs as templates may not yield correct results.

The narrowing of the active site observed in the P/CDK2/cyclinA/roscovitine was not found in the CDK5/p25/roscovitine complex. Furthermore, HBs that form between the glutamines and the inhibitors are different in both activated CDK2 and CDK5. These differences could provide an avenue in structure-based drug design for new structural inhibitors with improved selectivity between CDK2 and CDK5.

Acknowledgement Prof. Meijer Laurent in France and Dr. Sung-Hou KIM in University of Berkeley are gratefully acknowledged for generously offering the crystal structures of the CDK2/R-roscovitine complex.

References

1. Harper JW, Adams PD (2001) Chem Rev 101:2511
2. Garrett MD, Fattaey A (1999) Curr Opin Genet Dev 9:104
3. Webster KR (1998) Expert Opin Investig Drugs 7:865
4. Nguyen MD, Julien JP (2003) Neurosignals 12:215
5. Lau LF, Ahlijanian MK (2003) Neurosignals 12:209
6. Smith PD, Crocker SJ, Jackson-Lewis V, Jordan-Sciutto KL, Hayley S (2003) Proc Natl Acad Sci USA 100:13650
7. Bu B, Li J, Davies P, Vincent I (2002) J Neurosci 22:6515
8. Wang J, Liu S, Fu Y, Wang JH, Lu Y (2003) Nat Neurosci 6:1039
9. Hunter T, Pines J (1994) Cell 79:573
10. Sherr C (1996) Science 274:1672
11. Norbury C, Nurse P (1992) Annu Rev Biochem 61:441
12. De Azevedo WF Jr, Mueller-Dieckmann HJ, Schulze-Gahmen U, Worland PJ, Sausville E, Kim SH (1996) Proc Natl Acad Sci USA 93:2735
13. De Azevedo WF Jr, Leclerc S, Meijer L, Havlicek L, Strnad M, Kim SH (1997) Eur J Biochem 243:518
14. Jeffrey PD, Russo AA, Polyak K, Gibbs E, Hurwitz J, Massague J, Pavletich NP (1995) Nature 376:313
15. Patrick GN, Zhou P, Kwon YT, Howley PM, Tsai L-H (1998) J Biol Chem 273:24057
16. Patrick GN, Zukerberg L, Nikolic M, de la Monte S, Dikkes P, Tsai L-H (1999) Nature 402:615
17. Tarricone C, Dhavan R, Peng J, Areces LB, Tsai L-H, Musacchio A (2001) Mol Cell 8:657
18. Russo A, Jeffrey PD, Pavletich NP (1996) Nat Struct Biol 3:696
19. Morgan DO (1996) Curr Opin Cell Biol 8:767
20. Cavalli A, Dezi C, Folkers G, Scapozza L, Recanatini M (2001) Proteins Struct Funct Genet 45:478
21. Otyepka M, Kříž Z, Koča J (2002) J Biomol Struct Dyn 20:141
22. De Azevedo WF Jr, Gaspar RT, Canduri F, Camera JC Jr, Silveira NJF (2002) Biochem Biophys Res Commun 297:1154
23. Cavalli A, Vivo MD, Recanatini M (2003) Chem Commum 1308
24. Sims PA, Wong CF, McCammon JA (2003) J Med Chem 46:3314
25. Park H, Yeom MS, Lee S (2004) ChemBioChem 5:1662
26. Bártová I, Otyepka M, Kříž Z, Koča (2004) Protein Sci 13:1449
27. Bártová I, Otyepka M, Kříž Z, Koča J (2005) Protein Sci 14:445
28. Jiang Y-J, Zou J-W, Gui C-S (2005) J Mol Model 11:509
29. García-Sosa AT, Mancera RL (2006) J Mol Model 12:422
30. Davies TG, Tunnah P, Meijer L, Marko D, Eisenbrand G, Endicott JA, Noble MEM (2001) Structure 9:389
31. Leclerc S, Garnier M, Hoessel R, Marko D, Bibb JA, Snyder GL, Greengard P, Biernati J, Wui Y-Z, Mandelkowi E-M, Eisenbrand G, Meijer L (2001) J Biol Chem 276:251
32. Sausville EA (2002) Trends Mol Med 8:S32
33. Noble MEM, Endicott JA, Johnson LN (2004) Science 303:1800
34. Noble M, Barrett P, Endicott J, Johnson L, McDonnell J, Robertson G, Zawaira A (2005) Biochimica et Biophysica Acta 1754:58
35. Huew A, Mazitschek R, Giannis A (2003) Angew Chem Int Ed 42:2122
36. Sielecki M, Boylan JF, Benfield PA, Trainor GL (2000) J Med Chem 43:1
37. Knockaert P, Greengard L, Meijer L (2002) Trends Pharmacol Sci 23:417
38. Lau LF, Seymour PA, Sanner MA, Schachter JB (2002) J Mol Neurosci 19:267
39. Crews CM, Mohan R (2000) Curr Opin Chem Biol 4:47
40. Meijer L, Borgne A, Mulner O, Chong JP, Blow JJ, Inagaki N (1997) Eur J Biochem 243:527
41. Ljungman M, Paulsen MT (2001) Mol Pharmacol 60:785
42. Bach S, Knockaert M, Reinhardt J, Lozach O, Schmitt S, Baratte B, Koken M, Coburn SP, Tang L, Jiang T, Liang DC, Galons H, Dierick JF, Pinna LA, Meggio F, Totzke F, Schachtele C, Lerman AS, Carnero A, Wan Y, Gray N, Meijer L (2005) J Biol Chem 280:31208
43. Cornell WD, Cieplak P, Bayly CI, Gould IR, Merz KM, Ferguson DM Jr, Spellmeyer DC, Fox T, Caldwell JW, Kollman PA (1995) J Am Chem Soc 117:5179
44. Besler BH, Merz KM, Kollman PA (1990) J Comput Chem 11:431
45. Fox T, Kollman PA (1998) J Phys Chem B 102:8070
46. Case DA, Pearlman DA, Caldwell JW, Cheatham TE III, Wang J, Ross WS, Simmerling CL, Darden TA, Merz KM, Stanton RV, Cheng AL, Vincent JJ, rowley M, Tsui V, Gohlke H, Radme RJ, Duan Y, Pitera J, Massova I, Seibel GL, Singh UC, Weiner PK, Kollman PA (2002) AMBER 7. University of California, San Francisco
47. Jorgensen WL, Chandrasekhar J, Madura JD, Impey RW, Klein ML (1983) J Chem Phys 79:926
48. Darden T, York D, Pedersen L (1993) J Chem Phys 98:10089
49. Ryckaert JP, Ciccotti G, Berendsen HJC (1977) J Comput Phys 23:327
50. Morris GM, Goodsell DS, Huey R, Hart WE, Halliday S, Belew R, Olson AJ (1999) Autodock Version 3.0.3. Molecular Graphics Laboratory, Department of Molecular Biology, The Scripps Research Institute
51. Morris GM, Goodsell DS, Halliday RS, Huey R, Hart WE, Belew RK, Olson AJ (1998) J Comput Chem 19:1639
52. Massova I, Kollman PA (2000) Perspect Drug Discov 18:113
53. Connolly ML (1983) J Appl Cryst 16:548
54. Sitkoff D, Sharp KA, Honig B (1994) J Phys Chem 98:1978
55. Lemaitre V, Ali R, Kim C, Watts A, Fischer WB (2004) FEBS Lett 563:75